Layer-Dependent Photoresponse of 2D MoS_2 Films Prepared by Pulsed Laser Deposition

Lei Jiao,[a] Wenjing Jie,[b, c] Zhibin Yang,[c] Yuehui Wang,[a] Zhengwei Chen,[a] Xiao Zhang,[a] Weihua Tang,[a] Zhenping Wu,[a,*] Jianhua Hao,[c,*]

[a] *State Key Laboratory of Information Photonics and Optical Communications & School of Science, Beijing University of Posts and Telecommunications, Beijing 100876, China.*
[b] *College of Chemistry and Materials Science, Sichuan Normal University, Chengdu, 610066, China*
[c] *Department of Applied Physics, The Hong Kong Polytechnic University, Hung Hom, Hong Kong P. R. China*

[*] E-mail: zhenpingwu@bupt.edu.cn (Z. P. WU), jh.hao@polyu.edu.hk (J. H. HAO)

Abstract:

Due to the layered structure and thickness-dependent bandgap of MoS_2, it is intriguing to investigate the layer-dependent performance of MoS_2 based photodetectors. In this work, centimeter-scale layered MoS_2 films with different layer number are achieved by using pulsed laser deposition by controlling the number of laser pulses. The measurement of transport characteristics under dark indicates a Schottky barrier contact formed at Au/MoS_2 interface. The obtained metal-semiconductor-metal MoS_2 based photodetectors present a UV-to-NIR photoresponse with high stability. When decreasing the thickness of film, the photoresponse of the MoS_2 photodetectors is gradually increased from multilayer to bilayer, and more importantly, a notably enhanced in the photoresponse for monolayer can be observed. In particular, a photoresponsivity of 1.96 A/W is achieved in monolayer MoS_2 sample under an illumination with the wavelength of 300 nm. The physical mechanism responsible for the observation is discussed based on the layer dependent Schottky barrier variation and the indirect-to-direct energy band transition in MoS_2. Our work provides an insight into layer-dependent optical behavior in MoS_2 films, which should be helpful for developing further large-scale photosensing applications in the atomical limit.

Introduction

Atomically layered two-dimensional (2D) materials, largely owing to their novel electrical, optical, thermal and mechanical properties, are intriguing for both fundamental study and practical applications.[1-7] As a prototypical transition metal dichalcogenides (TMDs), MoS_2 is one of the most extensively studied 2D materials beyond graphene.[2-4, 8-19] Splendiani *et al.* reported a strong photoluminescence emerges from d-electrons' interactions,[20] in agreement of *ab initio* calculations,[21] indicating an indirect to direct energy band transition in MoS_2 monolayer. In particular, 2D MoS_2 crystals have a layer-dependent bandgap from 1.3 to 1.8 eV when thinning them from bulk to monolayer. Such features provide an ideal platform for establishing a variety of next generation electronic and optoelectronic devices in the 2D limit.[2, 22, 23]

In general, large-scale, high quality MoS_2 films are desired to meet the requirements for practical applications. Up to now, there are several techniques to prepare 2D materials, such as micro-mechanical exfoliation,[3, 15, 24] chemical exfoliation,[11] chemical vapor deposition (CVD),[25-29] magnetron sputtering,[30] atomic layer deposition,[31] spin-coating,[32] pulsed laser deposition (PLD),[33-38] and so on. Among them, PLD utilizes pure physical bottom-up method to prepare large scale thin films mainly under higher vacuum, which enables stoichiometry transferring from target to the film.[39] By taking advantages of precisely controlling of thickness through varying the laser pulses numbers, 2D materials with different layer numbers can be well prepared. Moreover, 2D films fabricated *via* PLD is appealing as an alternative with merits of good adhesion with substrate, fast growth speed and relatively low growth temperature compared to other techniques. Up to now, PLD method has successfully been used to grow large-scale 2D layered materials, such as MoS_2, amorphous black phosphorus (BP) and InSe, exhibiting unique features and good transport properties.[33-36, 40-42] Loh et al. reported to grow highly crystalline 2H-MoS_2 layers on Ag substrates, where a layer of formed Ag_2S at interface could become an excellent template to reduce the lattice mismatch.[43] Highly stoichiometry mono- and few- layer MoS_2 films were deposited on conventional substrates (Al_2O_3, HfO_2, quartz and SiO_2) by Serna and co-workers.[44] Their work

confirmed that the thickness of MoS_2 films can be accurately tuned by simply manipulating the laser repetition numbers. Serval studies have revealed that practical devices could be realized based on PLD grown MoS_2 films. Back-gate field-effect transistors were constructed by growing few-layer MoS_2 on Si substrates.[45] A flexible lateral p-n homogenous photodiode was also obtained based on monolayer MoS_2, where 619 % enhancement of photoresponsivity is achieved by utilizing external strain.[46] Although photoconductivity in different thickness mechanical exfoliated MoS_2 is studied using photocurrent spectral atomic force microscopy technique,[15] a systematical study of the layer-dependent photoresponse behaviors in large-scale MoS_2 devices is still desired, both for understanding the underlying mechanism and paving the way for potential optoelectronic applications.

In this work, centimeter-scale MoS_2 films ranging from 1L to 14L were prepared by using PLD method to study the layer-dependent photoresponse. All MoS_2 films based photodetectors exhibit photodetection ranging from UV (300 nm), visible to near-infrared (NIR) (800 nm) spectra, and response speed of 96 ms. Especially, the photoresponse increases when decreasing layer number, where monolayer MoS_2 film shows the highest photoresponsivity of 1.96 A/W under illumination (λ= 300 nm). Our findings may provide a useful approach to further develop high performance photodetectors based on large-scale 2D materials.

Experimental

Sample Preparation: MoS_2 films with different thickness were grown on SiO_2 (300 nm)/Si substrates (10 mm $\times$10 mm) by PLD. A coherent KrF excimer laser (λ = 248 nm) with a pulse energy of 200 mJ, a pulse width of 20 ns, and a repetition rate of 5 Hz was used in the experiment. The laser spot size on target is 0.2 mm $\times$ 0.4 mm. The chamber was initially evacuated to a base pressure of $\sim 1 \times 10^{-5}$ Pa. The bulk MoS_2 target (CTM Co., Ltd, 99.99%) was placed 5 cm in front of the substrates. During the deposition process, both target and substrates were rotated to obtain a uniform film growth. MoS_2 thin films were deposited at a deposition vacuum of $\sim 3 \times 10^{-5}$ Pa and a growth temperature of 700 °C. The as-grown samples were then cooled down to room

temperature naturally in the high-vacuum chamber. The thickness of the MoS_2 samples was controlled by changing number of laser pulses.

Structure and Optical Properties Characterization: The crystallinity of the MoS_2 films was investigated by a Bruker D8 Advance X-ray diffraction (XRD). Atomic force microscope (AFM, DI Nanocope 8) was employed to characterize the surface morphology of the prepared MoS_2 layers. The top-view transmission electron microscopy (TEM) specimen was prepared with a transfer process using NaOH solution. The cross-sectional TEM specimen was prepared by applying FIB (JEOL JIB-4500) milling and lift-off technique. The obtained samples were then transferred onto a copper grid for TEM (Bruker Nano) characterization. The valences of Mo ions and S ions were analyzed by X-ray photoelectron spectroscopy (XPS). The charge-shift spectrum was calibrated using the fortuitous C 1s peak at 284.8 eV. Raman spectra were obtained by a high-resolution confocal μ-Raman system (Horiba, HR 800) equipped with 532 nm laser source.

Devices Fabrication and Photoresponse Measurement: 100 nm-thick interdigital patterned Au electrodes were deposited on the surface of MoS_2 films by sputtering method. The output characteristics and time-dependent photoresponse were measured by a Keithley 2450 equipped with micromanipulator probe station SM-4. A laser diode with a wavelength of 650 nm or a Xe lamp with a monochromator was employed as the light source for the photoresponse measurement. All the measurements were carried out in ambient at room temperature.

Results and Discussion

XRD was carried out to identify the crystallographic orientation of the as-grown 2D layered MoS_2 samples. Figure 1a demonstrates the typical θ-2θ scans of the MoS_2 film (5000 pulses) grown on SiO_2/Si substrate. The existence of strong (002) peak indicates a highly out-of-plane textured MoS_2 films. The surface morphology of MoS_2 by AFM is shown in the inset of Figure 1a, suggesting a continuous and flat layer with the root-mean-square (RMS) roughness value of 0.227 nm, which is compatiable with the

reported CVD grown MoS_2 samples [47]. Furthermore, the stoichiometry and the chemical states of MoS_2 sample were characterized by using XPS. Figure 1b presents the Mo and S core-level peak regions of the MoS_2 film (360 pulses). It is noted that each of the Mo 3d and S 2p peaks can be fitted into well-defined doublet peaks. The Mo 3d spectrum presents two symmetrical peaks located at 228.8 eV and 231.9 eV, which are attributed to the binding states of Mo $3d_{5/2}$ and Mo $3d_{3/2}$ with a spin-orbit split differences of 3.1 eV. These results are consistent with the previously reported values to the Mo^{4+} state in MoS_2 film.[36] A small Mo^{6+} state peak (located near 235.1 eV) was observed, which probably caused by surface Mo-O bonding or oxidation in air.[30] The atomic ratio of Mo and S calculated from the ratio of the fitted peak areas in the XPS spectral. The result shows that the Mo:S ratio is ~1:1.96, which is very close to the chemical composition of the single dichalcogenide phase MoS_2. The stoichiometry of MoS_2 film can also be confirmed ~1:2 by the binding energy separation of 67.2 eV between the Mo $3d_{5/2}$ (228.8 eV) and S $2p_{3/2}$ (161.6 eV) peaks.[48] The top-view TEM image for the MoS_2 sample is shown in Figure 1c, revealing the periodic atom arrangement of the sample. Lattices with the spacing of 0.27 nm and 0.16 nm can be assigned to the (100) and (110) planes of the MoS_2, respectively. Both (100) and (110) planes can be well seen in the corresponding fast Fourier transform (FFT) pattern, as shown the inset of Figure 1c. The polycrystalline MoS_2 layers are evident by the approximate-circle patterns for both planes. Therefore, our MoS_2 layers are (001)-oriented with random in-plane orientation. The primary merit of employing PLD is the convenience to precisely control the MoS_2 layer numbers by simply changing the pulses numbers. Then, the layered structure nature and layer number of the fabricated MoS_2 samples can be confirmed by TEM. Figure 1d displays the cross-sectional TEM image of MoS_2 films via 360 pulses growth. A well-defined tri-layered structure was observed, with an interlayer spacing ~0.68 nm. This value is close to the theoretically calculated thickness for monolayer MoS_2 (~0.65 nm).[8, 9] Accordingly, the deposition rate of PLD-grown MoS_2 can be calculated based on the 120 laser pulses per monolayer.

Raman spectroscopy was used to estimate the layer numbers as well as the lattice

vibration modes of the prepared 2D layered MoS_2.[11, 49] Figure 2a demonstrates the Raman spectra of the MoS_2 films fabricated on SiO_2/Si substrates with different pulses numbers (120, 240, 360, 480, and 600). Here, a 532 nm laser was used to excite the resonant transition in MoS_2. There are two Raman peaks located near 407 cm^{-1} and 381 cm^{-1}, corresponding to the A_{1g} and E^1_{2g} vibration modes in MoS_2. The A_{1g} vibration serves as the result that S atomic sheets vibrate out-of-plane oppositely to Mo atomic sheets, while the E^1_{2g} vibration results from in-plane atoms vibration with an adverse direction for S and Mo atomic layers. Generally, the separation difference Δf between E^1_{2g} and A_{1g} peaks is in proportion to the layer number of MoS_2, following an empirical formula, $\Delta f = 26.45 - \frac{15.42}{1+1.44n^{0.9}}$ cm^{-1}. As shown in Figure 2a, with increasing of thickness of MoS_2, the E^1_{2g} peak exhibits a red shift while the A_{1g} peak shows a blue shift. The Δf was found to be 18.2 cm^{-1}, 21.2 cm^{-1}, 22.4 cm^{-1}, 23.5 cm^{-1}, and 25.1 cm^{-1} for the pulses numbers increased from 120 pulses to 600 pulses, respectively, revealing that the layer number of the obtained MoS_2 series is from 1L to 5L.[9] Thus, the growth rate by PLD method can be estimated according to the 120 laser pulses per monolayer, which is consistent with the aforementioned TEM results. Both Raman and TEM results suggest that the layer numbers of MoS_2 films can be accurately regulated by controlling the pulses number. To check the uniformity of the as-grown MoS_2 films, the Raman spectra were also used to examine on the four spots randomly selected from 5L MoS_2 film (Figure 2b). The bottom-right panel of Figure 2b demonstrates the microscopy image of the fabricated MoS_2 film with different spots where Raman spectra are accordingly shown in Figure 2b. Raman mapping image of 5L MoS_2 sample were also displayed over an area of 10 μm × 10 μm in the top-right panel of Figure 2b. The similar Δf values between E^1_{2g} peak and A_{1g} peak indicate that the films are highly homogeneous across a large-scale, which further confirms that large-scale 2D MoS_2 films with well-designed layer number can be well prepared by PLD.

For the measurement of optoelectronic properties, the metal-semiconductor-metal (MSM) structure based photodetectors were constructed by depositing three pairs of interdigital Au electrodes on top of the MoS_2 films by using a shadow mask, as

schematically shown in Figure 3a. The size of electrode fingers was 200 μm wide, 2800 μm long, and 200 μm spacing gap. Thus, the effective irradiated area for the obtained devices was ~0.062 cm^2, which is much larger than that of the photodetectors based on mechanical exfoliation flakes. The electronic affinity (E_{ea}) of MoS_2 layers is generally range from 4.0 eV for bulk to 4.5 eV for 1L.[15, 50] Therefore, with a work function $\Phi_{Au} \approx 5.1$ eV, the Au electrodes are expected to form a Schottky contact with MoS_2 layers. According to the Schottky-Mott theory, the corresponding Schottky barrier heights (Φ_B) could be estimated using equation $\Phi_B = \Phi_{Au} - E_{ea}$, resulting 0.6 eV for 1L up to 1.1 eV for bulk, respectively. To examine the Schottky junction properties, the curves of current as a function of the voltage (*I-V*) are recorded for MoS_2 films with layer number ranging from 1L to 4L. The *I-V* characteristics of the MoS_2 films are presented in Figure 3b. For 4L samples, a rectifying behavior is observed, confirming the Schottky-type contact at Au/MoS_2 interface. For 1L to 3L samples, the measured *I-V* behavior exhibits a rectify regime at low bias voltages and a wide saturation regime at high voltage. The *I-V* saturation occurred in MoS_2 could be attributed to pinch-off of the conducting band, which is one of essential characteristics for the future electronic applications.[3]

Based on the MSM structure, a typical photodetector can be constructed when the device is illuminated by external light sources. Photoresponsivity (*R*) is one of the significant parameters to determine the performance of optoelectronic devices, which are calculated by using the following equation:

$$R = (I_{photo} - I_{dark})/PS,$$

where *P* is the light intensity, *S* is the effective illuminated area.[51, 52] For simplicity, the photocurrent (I_{ph}) is defined as the absolute value of the current between dark and light illumination ($I_{ph} = I_{photo} - I_{dark}$). Figure 4a shows the photoresponsivity of monolayer MoS_2, which is illuminated by light in the spectral range from 300 to 900 nm. It is noticeable that as the wavelength of incident light increases from 300 to 650 nm, the photoresponsivity decreases from 1.96 A/W to 0.78 A/W, and is negligible at

wavelengths longer than 800 nm, which is in agreement with the direct bandgap of the MoS_2 monolayer.[8, 11, 53] The above results reveal that the MoS_2 films show a UV-to-NIR photoresponse, suggesting that PLD fabricated MoS_2 films are very attractive for broad spectral photodetection. Figure 4b shows the power dependence of the I_{ph} with the incident light of 650 nm. The I_{ph} increases significantly with increasing the incident light density range from 100 μW/cm^2 to 1 mW/cm^2, suggesting the photoresponse of the monolayer MoS_2 sample is notably controlled by the light intensity. To further understand the photoresponse of monolayer MoS_2, the I_{ph} and photoresponsivity as a function of light intensity with log-log scale are plotted in Figure 4c under the bias voltage of 1 V and incident light of 650 nm. It is found that the I_{ph} increases linearly as the power of incident light increases. And a nearly 1 of slope can be achieved for the photocurrent curve in log-log scale, suggesting the linear relationship between the photocurrent and the light intensity. It should be noted that the photoresponsivity shows a slight decrease when the incident power is increased, which might due to the trap states within MoS_2 film or near the MoS_2/Au interfaces.[49] It is observed that the MoS_2 monolayer obtained a high photoresponsivity of 1.32 A/W under relatively low light intensity (50 μW/cm^2). In order to further evaluate the photoresponse of monolayer MoS_2, the visible light (650 nm, 500 μW/cm^2) which is periodically switching between ON/OFF states was employed in our experiments. A bias of 1 V is applied on the MoS_2 films to separate photo-excited charge carriers. Figure 4d shows the time-dependent photoresponse of the MoS_2 photodetector under the periodical light illuminations. The current increases rapidly from 42.1 μA to 67.3 μA when the illumination light is turned on. After multiple cycles, the device still exhibits a nearly identical response, the stable and reversible switching between ON/OFF states of the device can imply the high robustness and good reproducibility of the photodetector.

Furthermore, the layer-dependent behaviors of MoS_2 based photodetectors are demonstrated. Figure 5a shows the layer-dependent time-resolved photocurrent under multiple illumination cycles. The photocurrent for all the three MoS_2 layers changes simultaneously with the ON/OFF states of the illumination light. Compared to few-

layer samples (4L: $I_{ph} \approx 8.5\ \mu A$, 3L: $I_{ph} \approx 12.4\ \mu A$), a much stronger response is obtained in the monolayer sample ($I_{ph} \approx 25.2\ \mu A$). Based on the time-resolved photoresponse plot of Figure 5a, the I_{ph} was found to strongly depend on the layer number of the MoS_2 films. To further understand the layer-dependent photoresponse, the I_{ph} as a function of layer number is plotted in Figure 5b, where error bars indicate the samples deviation. The curve can be divided into two stages, the initial decease from monolayer to 5L and then followed by the steady stage with thickness in excess of 5L up to 14L. In the process of the initial stage, the photoresponse of the MoS_2 photodetectors is gradually increased from multilayer to bilayer, and more importantly, a notably enhanced in the photoresponse for monolayer can be observed. Figure 5c presents the temporal response with a higher resolution of the photodetector during one circle of the incident periodical light. Both the rising and decay response times are measured to be around 96 ms for MoS_2 films with different layer numbers. Table 1 presents a comparison of the photoresponse parameters between our work and other reported 2D-material-based photodetectors. Our device shows a moderate responsivity and response time comparable to many reported photodetectors made from mechanical exfoliated films or CVD grown 2D materials.[10, 41, 54, 55] To understand the layer-dependence photoresponse in MoS_2 films, the Schottky barrier change near the Au/MoS_2 interface has to be considered, as schematically shown in Figure 5d. Since there is no metallic agent between Au and MoS_2, besides the Schottky barrier, an additional tunnel barrier could also be formed due to the existence of a van der Waals gap.[56] Here, we attribute the possible photocurrent generation mechanism to the Schottky barrier driven photocurrent located at Au/MoS_2 contacts. The Schottky barrier could generate a local built-in electric field that separate the photoexcited carriers at the contacts and drives the carriers toward the electrode.[57] Previous reports found that the transport processes in metal/MoS_2 are mainly determined by the thermionic emission of carriers through the Schottky barrier.[15, 55, 58] Generally, the Schottky barrier at the interface plays an essential role in determining the photoresponse property of the device, where the efficiency of the excited charge carriers flow overcoming the barrier is determined by the amplitudes of effective Φ_B. Since the effective Φ_B in monolayer

MoS_2 is lower than in few-layer MoS_2, a largely improved photoresponse in monolayer MoS_2 is observed. As a consequence, the layer-dependent photoresponse initially decreases as thickness increases. On the other hand, the effects of further increase thickness on the electronic structure of MoS_2 are negligible. Therefore, the barrier height between Au/MoS_2 should keep constant with thickness further increased, resulting in a nearly unchanged photoresponse in 5L, 8L and 14L samples. Moreover, the indirect-to-direct energy band transition could be another possible reason for the notably enhanced photoresponse in monolayer MoS_2 sample.[9] Our findings are consistent with the previously reported values for the pristine MoS_2 flakes obtained by mechanical exfoliation approach.[49, 53]

Conclusion

In conclusion, our results unequivocally illustrate the synthesizing of centimeter-scale high-quality 2D layered MoS_2 films by PLD. The thicknesses of the as-grown films are controlled by varying the laser pulses numbers, which is evidenced by the cross-sectional TEM and the Raman spectra results, respectively. The MoS_2 photodetectors show a photoresponse ranging from UV, visible to NIR spectra with the response time of 96 ms. Moreover, a layer-dependent photoresponse is observed in MoS_2 film. The responsivity is steady when the thickness beyond 5L, while enhanced dramatically as the thickness decreasing to monolayer, where the responsivity can reach up to the value of 1.96 A/W under illumination of 300 nm. The observed enhancement is attributed to the Schottky barrier variation near the Au/MoS_2 interface and the indirect-to-direct bandgap transition. Our results based on large-scale MoS_2 film should be helpful for developing high-performance large-scale optoelectronic devices in the 2D limit.

Acknowledgments

This work was supported by the National Natural Science Foundation of China (No. 61604100, 11404029, 51572033 and 51172208), the Fund of State Key Laboratory of

Information Photonics and Optical Communications (BUPT), RGC GRF (No. PolyU 153281/16P), and the Fundamental Research Funds for the Central Universities.

Notes and references

1. F. Hehai and H. Weida, *Adv. Sci.*, 2017, **4**, 1700323.
2. Q. H. Wang, K. Kalantar-Zadeh, A. Kis, J. N. Coleman and M. S. Strano, *Nat. Nanotechnol.*, 2012, **7**, 699-712.
3. B. Radisavljevic, A. Radenovic, J. Brivio, V. Giacometti and A. Kis, *Nat. Nanotechnol.*, 2011, **6**, 147-150.
4. Y. Ding, N. Zhou, L. Gan, X. Yan, R. Wu, I. H. Abidi, A. Waleed, J. Pan, X. Ou, Q. Zhang, M. Zhuang, P. Wang, X. Pan, Z. Fan, T. Zhai and Z. Luo, *Nano Energy*, 2018, **49**, 200-208.
5. C. Gong, K. Hu, X. Wang, P. Wangyang, C. Yan, J. Chu, M. Liao, L. Dai, T. Zhai, C. Wang, L. Li and J. Xiong, *Adv. Funct. Mater.*, 2018, **28**, 1706559.
6. C. Yan, L. Gan, X. Zhou, J. Guo, W. Huang, J. Huang, B. Jin, J. Xiong, T. Zhai and Y. Li, *Adv. Funct. Mater.*, 2017, **27**, 1702918.
7. J. Chu, F. Wang, L. Yin, L. Lei, C. Yan, F. Wang, Y. Wen, Z. Wang, C. Jiang, L. Feng, J. Xiong, Y. Li and J. He, *Adv. Funct. Mater.*, 2017, **27**, 1701342.
8. K. F. Mak, C. Lee, J. Hone, J. Shan and T. F. Heinz, *Phys. Rev. Lett.*, 2010, **105**, 136805.
9. Q. H. Wang, K. Kalantar-Zadeh, A. Kis, J. N. Coleman and M. S. Strano, *Nat. Nanotechnol.*, 2012, **7**, 699-712.
10. O. Lopez-Sanchez, D. Lembke, M. Kayci, A. Radenovic and A. Kis, *Nat. Nanotechnol.*, 2013, **8**, 497-501.
11. G. Eda, H. Yamaguchi, D. Voiry, T. Fujita, M. Chen and M. Chhowalla, *Nano Lett.*, 2011, **11**, 5111-5116.
12. W. J. Jie, Z. B. Yang, G. X. Bai and J. H. Hao, *Adv Opt Mater*, 2018, **6**.
13. R. V. Kashid, D. J. Late, S. S. Chou, Y.-K. Huang, M. De, D. S. Joag, M. A. More and V. P. Dravid, *Small*, 2013, **9**, 2730-2734.
14. D. J. Late, B. Liu, H. S. S. R. Matte, C. N. R. Rao and V. P. Dravid, *Adv. Funct. Mater.*, 2012, **22**, 1894-1905.
15. Y. Son, Q. H. Wang, J. A. Paulson, C. J. Shih, A. G. Rajan, K. Tvrdy, S. Kim, B. Alfeeli, R. D. Braatz and M. S. Strano, *ACS Nano*, 2015, **9**, 2843-2855.
16. D. J. Late, Y.-K. Huang, B. Liu, J. Acharya, S. N. Shirodkar, J. Luo, A. Yan, D. Charles, U. V. Waghmare, V. P. Dravid and C. N. R. Rao, *ACS Nano*, 2013, **7**, 4879-4891.
17. D. J. Late, B. Liu, H. S. S. R. Matte, V. P. Dravid and C. N. R. Rao, *ACS Nano*, 2012, **6**, 5635-5641.
18. C. Gong, Y. Zhang, W. Chen, J. Chu, T. Lei, J. Pu, L. Dai, C. Wu, Y. Cheng, T. Zhai, L. Li and J. Xiong, *Adv. Sci.*, 2017, **4**, 1700231.
19. Y. Yang, N. Huo and J. Li, *J. Mater. Chem. C*, 2017, **5**, 11614-11619.
20. A. Splendiani, L. Sun, Y. B. Zhang, T. S. Li, J. Kim, C. Y. Chim, G. Galli and F. Wang, *Nano Lett.*, 2010, **10**, 1271-1275.
21. A. Ramasubramaniam, *Phys. Rev. B*, 2012, **86**, 115409.
22. P. Wangyang, C. Gong, G. Rao, K. Hu, X. Wang, C. Yan, L. Dai, C. Wu and J. Xiong, *Adv Opt Mater*, 2018, **6**, 1701302.
23. Z. Y. Yin, H. Li, H. Li, L. Jiang, Y. M. Shi, Y. H. Sun, G. Lu, Q. Zhang, X. D. Chen and H. Zhang, *Acs Nano*, 2012, **6**, 74-80.
24. D. Chakravarty and D. J. Late, *Eur. J. Inorg. Chem.*, 2015, **2015**, 1973-1980.
25. D. Kong, H. Wang, J. J. Cha, M. Pasta, K. J. Koski, J. Yao and Y. Cui, *Nano Lett.*, 2013, **13**, 1341-

1347.
26. G. Bai, S. Yuan, Y. Zhao, Z. Yang, S. Y. Choi, Y. Chai, S. F. Yu, S. P. Lau and J. Hao, *Adv. Mater.*, 2016, **28**, 7472-7477.
27. H. Yu, M. Liao, W. Zhao, G. Liu, X. J. Zhou, Z. Wei, X. Xu, K. Liu, Z. Hu, K. Deng, S. Zhou, J.-A. Shi, L. Gu, C. Shen, T. Zhang, L. Du, L. Xie, J. Zhu, W. Chen, R. Yang, D. Shi and G. Zhang, *ACS Nano*, 2017, **11**, 12001-12007.
28. A. S. Pawbake, M. S. Pawar, S. R. Jadkar and D. J. Late, *Nanoscale*, 2016, **8**, 3008-3018.
29. A. S. Pawbake, R. G. Waykar, D. J. Late and S. R. Jadkar, *Acs Appl Mater Inter*, 2016, **8**, 3359-3365.
30. J. Tao, J. Chai, X. Lu, L. M. Wong, T. I. Wong, J. Pan, Q. Xiong, D. Chi and S. Wang, *Nanoscale*, 2015, **7**, 2497-2503.
31. J. J. Pyeon, S. H. Kim, D. S. Jeong, S.-H. Baek, C.-Y. Kang, J.-S. Kim and S. K. Kim, *Nanoscale*, 2016, **8**, 10792-10798.
32. J. Yang, Y. Gu, E. Lee, H. Lee, S. H. Park, M.-H. Cho, Y. H. Kim, Y.-H. Kim and H. Kim, *Nanoscale*, 2015, **7**, 9311-9319.
33. M. I. Serna, S. H. Yoo, S. Moreno, Y. Xi, J. P. Oviedo, H. Choi, H. N. Alshareef, M. J. Kim, M. Minary-Jolandan and M. A. Quevedo-Lopez, *ACS Nano*, 2016, **10**, 6054-6061.
34. G. Siegel, Y. P. V. Subbaiah, M. C. Prestgard and A. Tiwari, *Apl Materials*, 2015, **3**, 056103.
35. C. R. Serrao, A. M. Diamond, S. L. Hsu, L. You, S. Gadgil, J. Clarkson, C. Carraro, R. Maboudian, C. M. Hu and S. Salahuddin, *Appl. Phys. Lett.*, 2015, **106**, 052101.
36. W. Jie, Z. Yang, F. Zhang, G. Bai, C. W. Leung and J. Hao, *ACS Nano*, 2017, **11**, 6950-6958.
37. M. Z. Bellus, Z. B. Yang, J. H. Hao, S. P. Lau and H. Zhao, *2d Materials*, 2017, **4**, 025063.
38. Z. B. Yang, J. H. Hao, S. G. Yuan, S. H. Lin, H. M. Yau, J. Y. Dai and S. P. Lau, *Adv. Mater.*, 2015, **27**, 3748-3754.
39. Z. P. Wu, W. Huang, K. H. Wong and J. H. Hao, *J. Appl. Phys.*, 2008, **104**, 054103.
40. T. A. Loh and D. H. Chua, *ACS Appl. Mater. Interfaces*, 2014, **6**, 15966-15971.
41. Z. Yang, W. Jie, C. H. Mak, S. Lin, H. Lin, X. Yang, F. Yan, S. P. Lau and J. Hao, *ACS Nano*, 2017, **11**, 4225-4236.
42. Z. B. Yang and J. H. Hao, *J. Mater. Chem. C*, 2016, **4**, 8859-8878.
43. T. A. J. Loh and D. H. C. Chua, *Chem. Phys. Lett.*, 2014, **610**, 284-287.
44. M. I. Serna, S. H. Yoo, S. Moreno, Y. Xi, J. P. Oviedo, H. Choi, H. N. Alshareef, M. J. Kim, M. Minary-Jolandan and M. A. Quevedo-Lopez, *Acs Nano*, 2016, **10**, 6054-6061.
45. L. Jiao, Y. Wang, Y. Zhi, W. Cui, Z. Chen, X. Zhang, W. Jie and Z. Wu, *Advances in Condensed Matter Physics*, 2018, **2018**, 3485380.
46. K. Zhang, J. Y. Zhai and Z. L. Wang, *2d Materials*, 2018, **5**.
47. X. Ling, Y.-H. Lee, Y. Lin, W. Fang, L. Yu, M. S. Dresselhaus and J. Kong, *Nano Lett.*, 2014, **14**, 464-472.
48. M. A. Baker, R. Gilmore, C. Lenardi and W. Gissler, *Appl. Surf. Sci.*, 1999, **150**, 255-262.
49. W. Zhang, J. K. Huang, C. H. Chen, Y. H. Chang, Y. J. Cheng and L. J. Li, *Adv. Mater.*, 2013, **25**, 3456-3461.
50. S. W. Han, H. Kwon, S. K. Kim, S. Ryu, W. S. Yun, D. H. Kim, J. H. Hwang, J. S. Kang, J. Baik, H. J. Shin and S. C. Hong, *Phys. Rev. B*, 2011, **84**, 045409.
51. S. R. Tamalampudi, Y. Y. Lu, U. R. Kumar, R. Sankar, C. D. Liao, B. K. Moorthy, C. H. Cheng, F. C. Chou and Y. T. Chen, *Nano Lett.*, 2014, **14**, 2800-2806.

52. S. Lei, X. Wang, B. Li, J. Kang, Y. He, A. George, L. Ge, Y. Gong, P. Dong, Z. Jin, G. Brunetto, W. Chen, Z. T. Lin, R. Baines, D. S. Galvao, J. Lou, E. Barrera, K. Banerjee, R. Vajtai and P. Ajayan, *Nat. Nanotechnol.*, 2016, **11**, 465-471.
53. D. S. Tsai, K. K. Liu, D. H. Lien, M. L. Tsai, C. F. Kang, C. A. Lin, L. J. Li and J. H. He, *ACS Nano*, 2013, **7**, 3905-3911.
54. W. Choi, M. Y. Cho, A. Konar, J. H. Lee, G. B. Cha, S. C. Hong, S. Kim, J. Kim, D. Jena, J. Joo and S. Kim, *Adv. Mater.*, 2012, **24**, 5832-5836.
55. H. S. Lee, S. W. Min, Y. G. Chang, M. K. Park, T. Nam, H. Kim, J. H. Kim, S. Ryu and S. Im, *Nano Lett.*, 2012, **12**, 3695-3700.
56. A. Allain, J. H. Kang, K. Banerjee and A. Kis, *Nat. Mater.*, 2015, **14**, 1195-1205.
57. H. Xu, J. Wu, Q. Feng, N. Mao, C. Wang and J. Zhang, *Small*, 2014, **10**, 2300-2306.
58. Y. Li, C. Y. Xu and L. Zhen, *Appl. Phys. Lett.*, 2013, **102**, 143110.

Table Caption:

Table 1. Comparison of the performance of the 2D-material-based photodetectors.

Figure Captions:

Figure 1. (a) XRD results of a PLD grown MoS_2 film. The inset presents the surface morphology of MoS_2 film by AFM. (b) XPS spectra of Mo 3d , S 2s and S 2p. (c) High-resolution TEM image of the MoS_2 film. (d) Cross-section TEM image of 3L MoS_2 film.

Figure 2. (a) Layer-dependent Raman spectra of MoS_2 films deposited on SiO_2/Si substrates with laser pulses number of 120, 240, 360, 480, and 600. (b) Raman spectra of four random spots on the MoS_2 films surface. Inset: Optical micrograph of four randomly selected spots.

Figure 3. (a) schematics of the photoresponse measurement geometry. (b) The *I-V* characteristics of the MoS_2 films.

Figure 4. Photoresponse of 1L MoS_2 (a) The wavelength selectivity ranging from 300 to 900 nm. (b) The light intensity dependence of photoresponse under 650 nm illumination. The *I-V* characteristic curves of the photodetector in the dark and under 650 nm light illumination with various light intensities (c) The light intensity dependence of photocurrent and responsivity. (d) Time-dependent photoresponse under 650 nm light on/off switching at 1 V.

Figure 5. (a) Time-dependent photoresponse of MoS_2 films with layer number of 1, 3, 4. (b) Plot of photocurrent as a function of MoS_2 layer number. Error bars indicate samples deviations. (c) The temporal response with a higher resolution of the MoS_2 photodetector during one circle of the incident periodical light. (d) Band diagram of MoS_2 photodetector.

Table 1

Photodetector	Method	Thickness	Spectral range (nm)	Responsivity (A/W)	Response time (ms)	Ref.
Au/MoS_2	exfoliation	1L	561	880	4000/9000	[10]
Au-Ti/MoS_2	exfoliation	1L	550	7.5×10^{-3}	50	[23]
Au-Ti/MoS_2	exfoliation	multilayer	450-850	> 0.1	-	[54]
Graphene/MoS_2	exfoliation	2L	400-1000	>10	280/150	[57]
Au-Ti/MoS_2	exfoliation	1L	635	10^6	few seconds	[19]
MoS2 p-n junction	CVD	1L	532	1162	tens of second	[46]
Au/InSe	PLD	3 nm	370-980	27	500/1700	[41]
Au/ MoS_2	PLD	1L	300-800	1.96	98/98	This work

Figure 1a, b, c, d

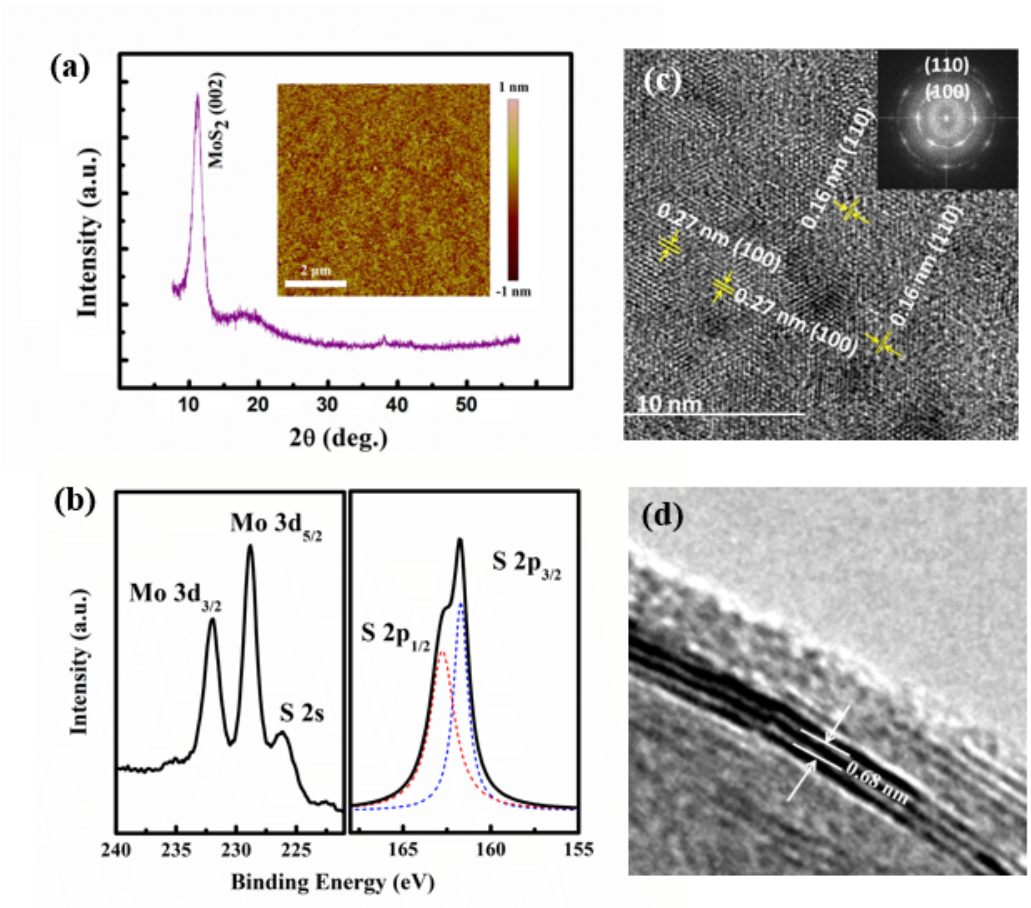

Figure 2a, b

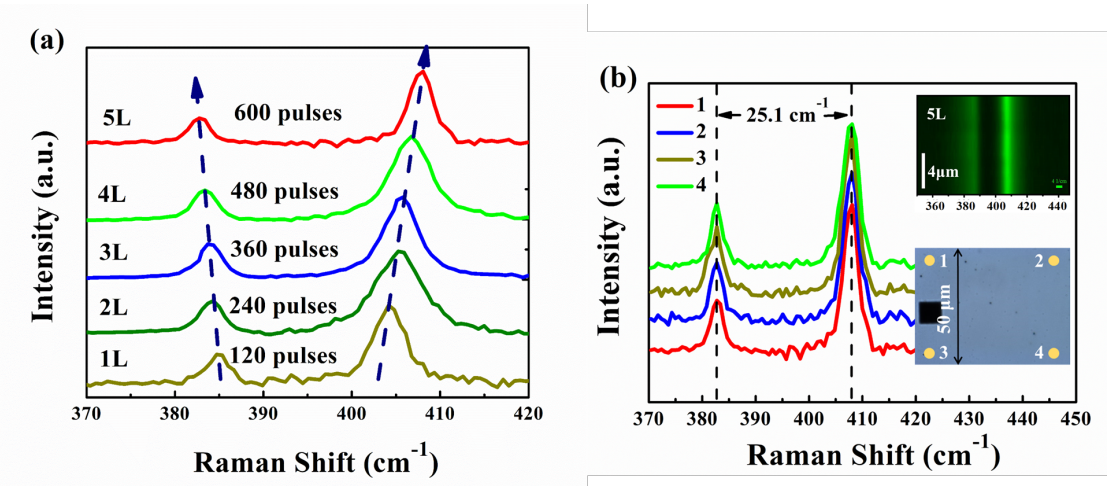

Figure 3a, b

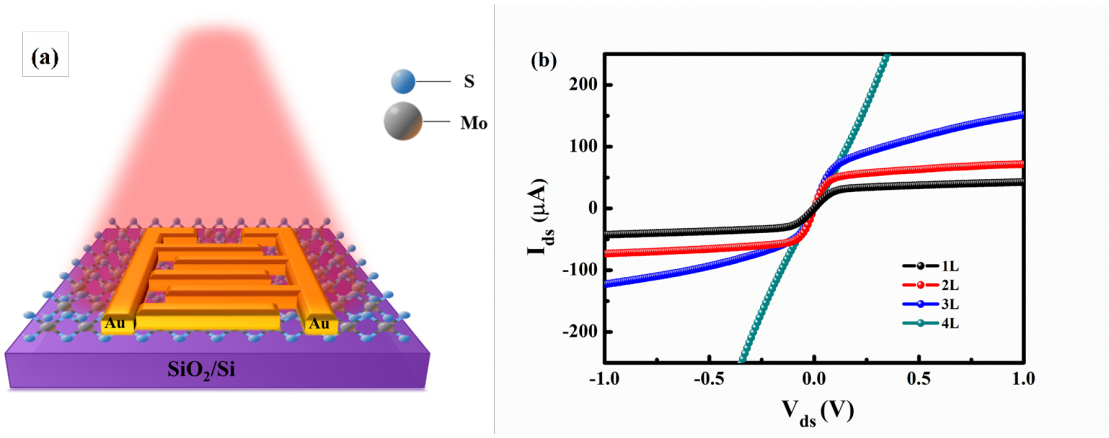

Figure 4a, b, c, d

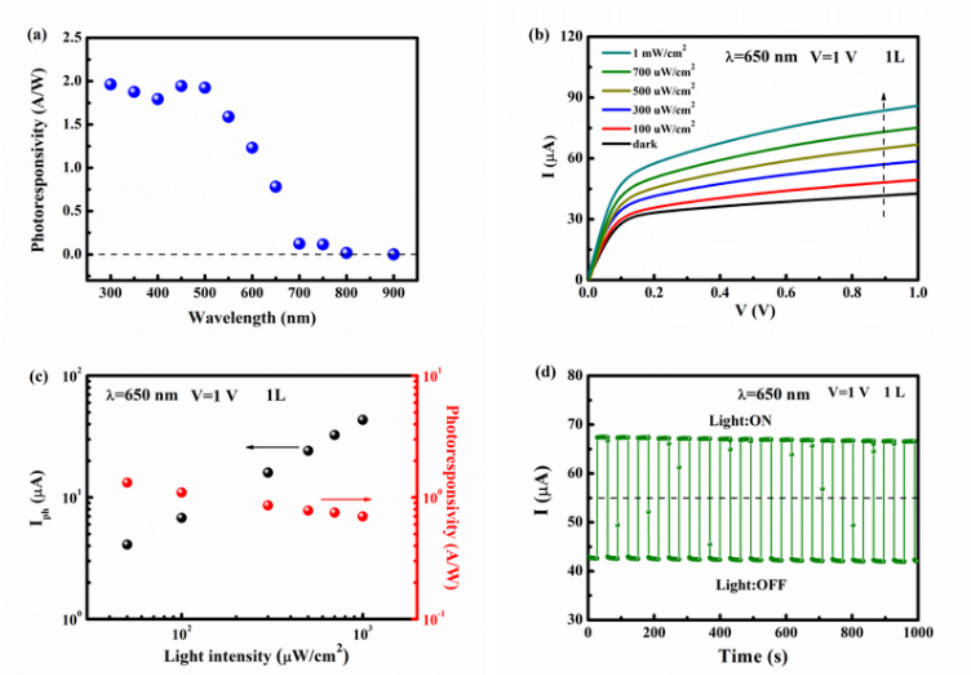

Fig 5a, b, c, d

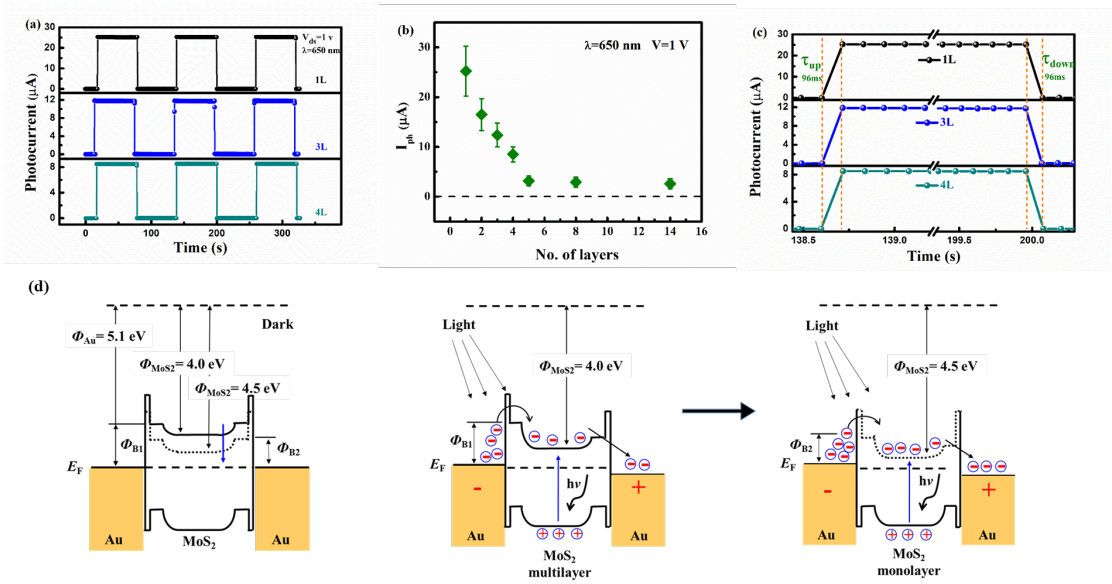
(a)
Photocurrent (μA)
Time (s)
1L
3L
4L
(b)
λ=650 nm V=1 V
I_{ph} (μA)
No. of layers
(c)
Photocurrent (μA)
Time (s)
1L
3L
4L
(d)
Dark
Φ_{Au}= 5.1 eV
Φ_{MoS2}= 4.0 eV
Φ_{MoS2}= 4.5 eV
Φ_{B1}
Φ_{B2}
E_F
Au
MoS_2
Au
Light
Φ_{MoS2}= 4.0 eV
hν
MoS_2 multilayer
Light
Φ_{MoS2}= 4.5 eV
hν
MoS_2 monolayer